frontiers | Frontiers in Materials

TYPE Original Research
PUBLISHED 18 July 2025
DOI 10.3389/fmats.2025.1596814

OPEN ACCESS

EDITED BY
Harikrishnan Pulikkalparambil,
Mahatma Gandhi University, India

REVIEWED BY
Syahrul Fithry Senin,
Universiti Teknologi Teknologi MARA, Cawangan Pulau Pinang, Malaysia
Sabarish Radoor,
Myongji University, Republic of Korea

*CORRESPONDENCE
Huan Xi,
357005578@qq.com,
xihuanhhu@163.com

RECEIVED 20 March 2025
ACCEPTED 25 June 2025
PUBLISHED 18 July 2025

CITATION
Xi H, Chang X, Sun T and Chen L (2025) Preparation and phosphate adsorption performance of La modified bentonite composite membrane.
Front. Mater. 12:1596814.
doi: 10.3389/fmats.2025.1596814

Preparation and phosphate adsorption performance of La modified bentonite composite membrane

Huan Xi [1]*, Xiangming Chang[2], Tingting Sun[1] and Liang Chen[1]

[1]College of Road, Bridge and Port-Harbor Engineering, Nanjing Vocational Institute of Transport Technology, Nanjing, China, [2]School of Physics and Technology, Wuhan University, Wuhan, China

Using selective adsorption membrane for low-concentration phosphate removal from water is one of the current research hotspots. In this study, La modified bentonite PVC membrane (abbreviated as PVC-LaBT) was prepared by chemical precipitation and phase conversion method. Compared to pure PVC membrane and PVC-BT (pure bentonite PVC membrane), PVC-LaBT shows more pores and larger surface roughness, which is due to the intercalation of La ions into the layers of bentonite, resulting in larger pure water flux and adsorption capacity. Using 1 $mg{\cdot}L^{-1}$ phosphate solution, after treatment of 8 h by PVC-LaBT, phosphate concentration decreased to 0.1 $mg{\cdot}L^{-1}$, significantly less than the phosphate concentrations of solution treated by PVC-BT (0.5 $mg{\cdot}L^{-1}$) and PVC (0.7 $mg{\cdot}L^{-1}$). At an initial phosphate concentration of 5.0 $mg{\cdot}L^{-1}$, the maximum adsorption capacity was measured as 242.86 $mg{\cdot}m^{-2}$. Acid solution is conducive to phosphate adsorption, while the phosphate adsorption performance under alkaline solution is poor. Some anions (Cl^- and NO_3^-) have little effects on phosphate adsorption, the others (SO_4^{2-} and CO_3^{2-}) can inhibit phosphate adsorption. This study synthesized a green membrane, providing a new strategy for low concentration phosphate removal.

KEYWORDS

bentonite, La intercalation, composite membrane, phosphate, adsorption

1 Introduction

The intensification of water eutrophication is a common environmental problem faced by mankind. Untreated industrial and agricultural wastewater, as well as domestic sewage, contain a large amount of nutrient element (Ahmadijokani et al., 2022). If they discharge and the phosphorus concentration of lakes and oceans exceeds 0.02 $mg{\cdot}L^{-1}$, it will lead to algae blooms, reduction of dissolved oxygen and death of animals and plants in the water, thus threaten human production and life through the food chain (Rangabhashiyam et al., 2022).

Traditional chemical precipitation method is affected by water pH, and produces a large amount of sludge (Di Capua et al., 2022). Biological method has water quality sensitivity, as well as disability of removing low concentration of phosphate (Zhang C. et al., 2022). Compared with them, adsorption method has the advantages

of high efficiency, environmental production and easy operation (Zhang M. et al., 2022; Radoor et al., 2024). The key to the effectiveness of adsorption method is the choice of adsorbent (Sabarish and Unnikrishnan, 2019).

Bentonite has abundant reserve, whose price is only about 1/20 of activated carbon. It has a large specific surface area and excellent ion exchange capacity, making it a commonly used raw material for water pollution adsorbent. Natural bentonite has negative charge on the surface, thus exhibits very low adsorption capacity for anionic pollutants (Wang B. et al., 2023). Metal elements such as iron, aluminum, lanthanum, zirconium and magnesium have been used as modifier (Liu et al., 2022). Compare with other metal ions, the efficiency of phosphate ion precipitation with lanthanum is higher in the wide pH range (4.5–8.5) (Mi et al., 2022). Based on this, the Australian Federal Scientific and Industrial Research Organization (CSIRO) has developed lanthanum modified bentonite (Phoslock®) in the 1990s and it has been used in more than 150 water bodies in more than 20 countries around the world (Dithmer et al., 2016).

However, on the one hand, the volume of bentonite expands after water adsorption, which is easy to form muddy mud. Then the water turbidity increases and it is difficult to form precipitation to recover bentonite. Granular bentonite leads to the decrease of specific surface area and porosity, leading to lower adsorption capacity (Haciosmanoglu et al., 2022). On the other hand, for the low concentration of phosphorus-containing wastewater, it is often difficult to meet the phosphate discharge standard of wastewater by adsorption method (Hnamte and Pulikkal, 2022). Based on the above situation, loading La modified bentonite into ultrafiltration membrane has the opportunity to capture low phosphate concentration by cross-flow filtration. There have been studies that utilized the combination of eco-friendly adsorbent and organic membrane for water treatment and achieved satisfactory results (Sabarish and Unnikrishnan, 2018; Radoor et al., 2025).

In this study, PVC-LaBT was prepared through La modification of bentonite and phase inversion method. Pure PVC membrane and PVC membrane loaded with natural bentonite were also prepared for performance comparison. The experiments showed that the addition of La modified bentonite increased the phosphate removal efficiency of the composite membrane by about 3 times. The novel PVC-LaBT also solved the solid-liquid separation problem during the adsorption process.

2 Materials and methods

2.1 Raw materials

Bentonite was supplied by Hebei Lingshou Dehang Mine Products Co. Ltd., China. Chemically pure $La(NO_3)_3{\cdot}6H_2O$, NaOH, polyvinyl chloride (PVC), N-methyl-2-pyrrolidone (NMP) and other chemicals were analytical grade and supplied by Sino pharm Chemical Reagent Co., Ltd., China. Dried KH_2PO_4 was used for preparing phosphate stock solution (1,000 $mg{\cdot}L^{-1}$). The working solutions of experiments were prepared by diluting above stock solution.

2.2 Preparation of PVC-LaBT

Preparation of LaBT: First, 25 g of bentonite was added into 250 mL of 2% La^{3+} solution and stirred magnetically for 3 h at room temperature. Next, the pH of the mixture was adjusted to about 8.0 by 1 $mol{\cdot}L^{-1}$ of NaOH solution, and then the mixture was stirred for another 2 h for sufficient precipitation reaction. Then, the solid particles were obtained by centrifugation at 8,000 rpm, washed three times and dried in a vacuum oven at 60°C. Finally, the solid particles were ground, screened through 200 mesh, labeled as LaBT and store for usage.

Preparation of La modified bentonite doped PVC membrane (PVC-LaBT) (Xi et al., 2023; Zhang et al., 2024): First, 5 g of LaBT was slowly added to 45 g of NMP. The mixture was magnetically stirred for 2 h at room temperature to form a stable suspension. Then, 5.0 g of PVC was slowly added to the suspension with magnetic stirring for 5 h until PVC was completely dissolved. Then

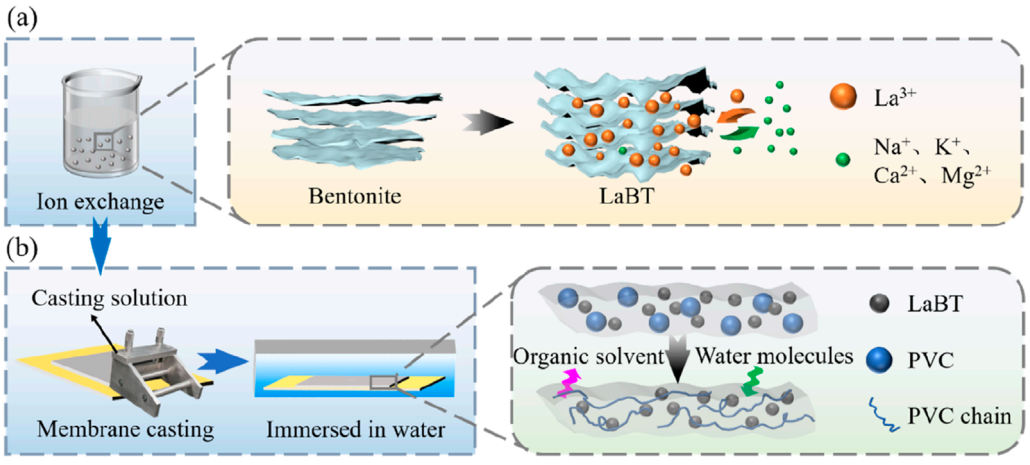

FIGURE 1
Illustration for the fabrication process of **(a)** LaBT and **(b)** PVC-LaBT.

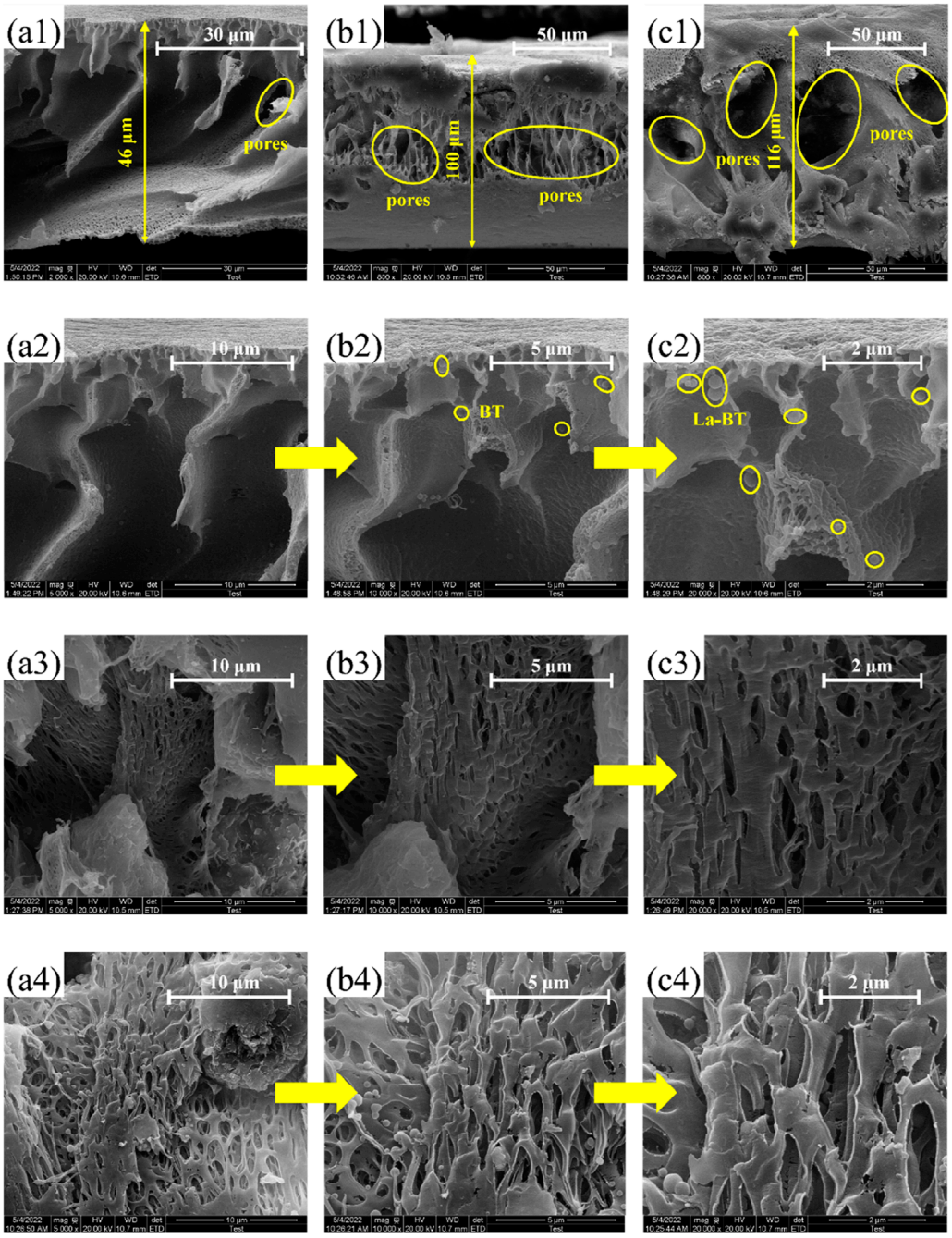

FIGURE 2
The SEM images of cross sections of **(a1-a4)** PVC, **(b1-b4)** PVC-BT and **(c1-c4)** PVC-LaBT.

it was sonicated for 1 h and vacuum degassed for 0.5 h to remove bubbles in the solution. After that, the adjustable casting device was set to 200 μm, placed on the automatic casting machine and casted the mixed solution on the smooth glass plate (Xi et al., 2023; Zhang et al., 2024). Then the glass plate was immediately put into pure water to form membrane. It was placed in pure water for 24 h to ensure sufficient solvent replacement. Finally, the prepared membrane was naturally dried and labeled as PVC-LaBT for further experiments. The preparation method of PVC-LaBT is shown in Figure 1.

In addition, the pure PVC membrane (PVC) and the PVC membrane supplemented with unmodified bentonite (PVC-BT) were prepared in the same way for comparation.

2.3 Microstructural characterization

In this experiment, the microstructural characterizations of as-obtained membranes were analyzed by scanning electron microscopy (SEM) and atomic force microscope (AFM).

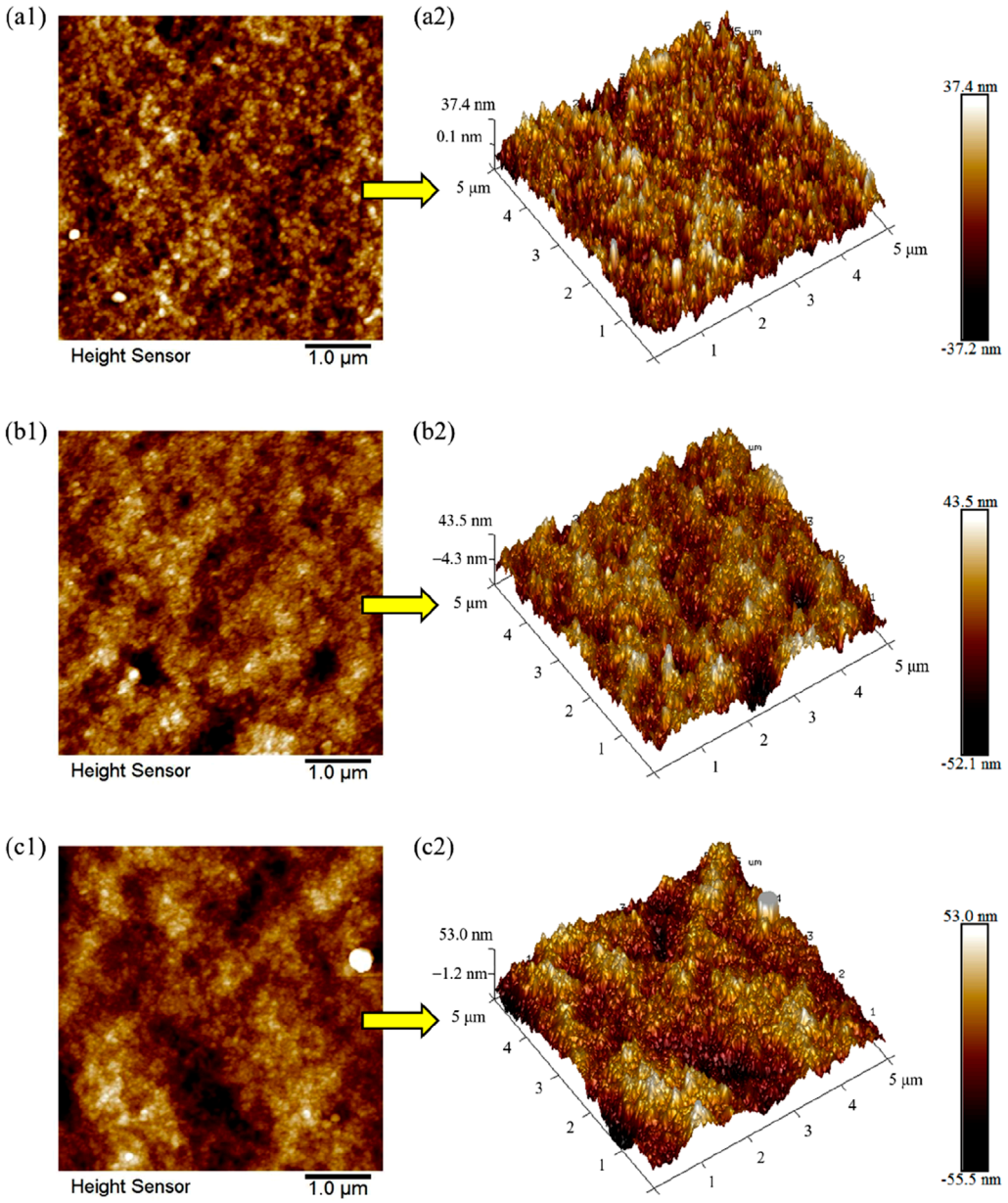

FIGURE 3
2D and 3D AFM test images of **(a1, a2)** PVC membrane, **(b1, b2)** PVC-BT membrane and **(c1, c2)** PVC-LaBT membrane.

TABLE 1 Surface roughness information of three membranes.

Membrane sample	Ra (nm)	Rq (nm)	Rmax (nm)
PVC	8.5	10.7	90.3
PVC-BT	9.7	12.6	122.0
PVC-LaBT	12.2	15.7	170.0

The field emission scanning electron microscope (Hitachi Regulus-8100, Japan) was used to analyze the microscopic morphology of the sample sections. The acceleration voltage was 15 kV and the ratio was 15–60,000 times. The processing requirements of the membrane sample are as follows. The three kinds of membrane samples were pulled off by hand or cut with scissors, and then sprayed with gold. The sample sections were scanned at different magnifications to obtain the SEM images of the membrane sample sections. The microscopic morphologies, pore structures and approximate thickness of the membrane samples can be analyzed.

The roughness of the membranes was characterized by atomic force microscope (AFM, Bruker Dimension Icon, America). Roughness is the key index to measure the surface fluctuation degree of the membrane material. Usually, the greater the roughness of the membrane, the better its adsorption performance. In this study, the atomic force microscope scanning images of the composite

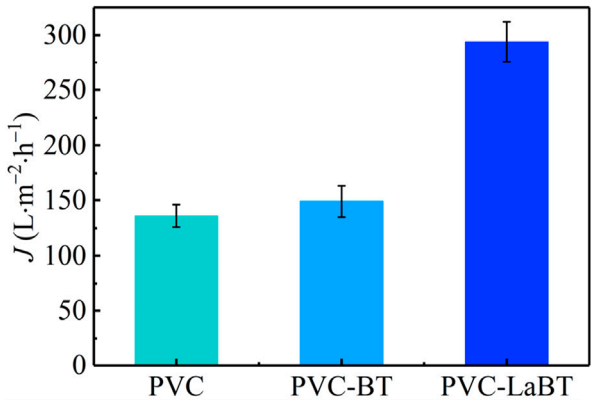

FIGURE 4
Pure water flux of three membranes.

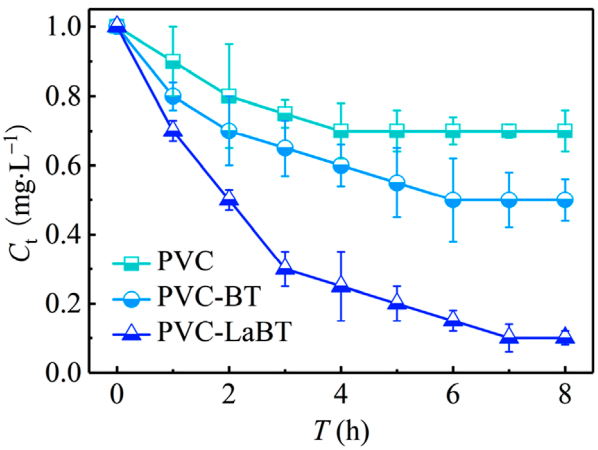

FIGURE 5
Phosphate concentration over time treated by different membranes.

membranes were obtained, and the average roughness (Ra) and the root mean square roughness (Rq) of the membrane surfaces were analyzed.

2.4 Performance testing

In this study, the adsorption and filtration properties of as obtained membranes were tested with the triple high pressure plate membrane testing equipment. The effective membrane area was 70 cm^2. The frequency of the triple high pressure plate membrane testing equipment was adjusted to 10 Hz. The solution filtration volume per unit of time were measured without applied pressure and the pure water flux (J, $L{\cdot}m^{-2}{\cdot}h^{-1}$) of the composite membranes was calculated by the following Equation 1.

$$J = \frac{V}{S \cdot \Delta t} \tag{1}$$

where V is the filtration volume (L), S is the effective area of membrane filtration (m^2) and Δt is the filtration time (h).

The phosphate stock solution was diluted to different concentrations (1 $mg{\cdot}L^{-1}$ and 5 $mg{\cdot}L^{-1}$). 3000 mL of diluted phosphate solution was added to the water tank of the equipment at room temperature (25°C). Then the frequency was adjusted to 10 Hz. The solution was cycled through cross flow mode without applied pressure. 10 mL of water samples were taken at certain intervals, and the phosphate concentrations were detected through phosphorus-molybdenum blue spectrophotometry. In addition, the effects of different pH and coexisting salt ions on the phosphate adsorption performance of PVC-LaBT were analyzed.

The equilibrium adsorption capacity (q_e, $mg{\cdot}m^{-2}$) and adsorption capacity at time t (q_t, $mg{\cdot}m^{-2}$) were calculated by using the Equations 2, 3 respectively below:

$$q_e = \frac{(C_0 - C_e)V}{S} \tag{2}$$

$$q_t = \frac{(C_0 - C_t)V}{S} \tag{3}$$

where C_0 ($mg{\cdot}L^{-1}$), C_e ($mg{\cdot}L^{-1}$), and C_t ($mg{\cdot}L^{-1}$) are initial phosphate concentration, equilibrium phosphate concentration and phosphate concentration at time t (h), V is the filtration volume (L) and S is the effective area of membrane filtration (m^2).

3 Results and discussion

3.1 Characterization of prepared membranes

3.1.1 SEM images

To compare the internal microstructures of PVC, PVC-BT and PVC-LaBT, cross sections of these membranes are shown in Figure 2.

As can be seen from Figures 2a1–c1, the thickness of PVC membrane is about 50 μm, while that of PVC-BT and PVC-LaBT were 100 μm and 116 μm respectively. All three membranes were prepared by 200 μm applicator, but the thickness of the finished membranes is less than 200 μm. This is because the membranes shrunk during the process of phase conversion. During the experiment, we also optimized the thickness of the membrane. When the thickness was 100 or 150 μm, the membrane was prone to breakage during the casting process, and small holes were likely to appear on the membrane surface. When the thickness exceeded 200 μm, due to the high fluidity of the casting solution, the scraper was unable to evenly smooth the surface of the membrane.

Furthermore, the addition of adsorbent increased the viscosity of PVC solution, which reduced the contraction space of the membrane during phase conversion process. Therefore, the thickness of PVC-BT and PVC-LaBT is larger than that of pure PVC membrane.

By observing the structure of the membrane sections, it can be seen that there are some channels in PVC membrane, but the number and size are both small. The cross section of PVC-BT shows a mesh structure, but the pore size is small. There are numerous of pores with large size distributes in the internal of PVC-LaBT.

To compare the internal microstructures of PVC, PVC-BT and PVC-LaBT, cross sections of the three membranes were visualized

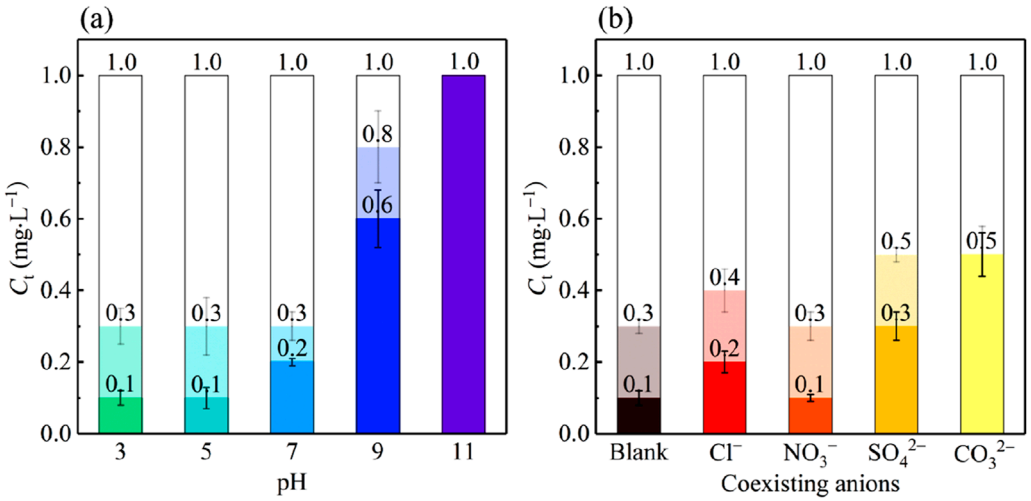

FIGURE 6
C_t after 4 h and 8 h under the influence of **(a)** pH and **(b)** coexisting anions.

TABLE 2 Similar membranes comparison for phosphate adsorption.

Membrane	EM[a]	Pressure (bar)	Water flux (L·m^{-2}·h^{-1})	pH	T[b] (°C)	IC[c] (mg·L^{-1})	AD[d]
La-based nanofiber membrane (Jia et al., 2022)	Batch adsorption	—	—	4–10	15–45	1–100	50 mg.g^{-1}
UiO-66(Zr)-NH2/PVC membrane (Pan et al., 2022a)	Adsorptive ultrafiltration	1	267	3–9	25	10	30 mg.g^{-1}
LC@MWCNTs membrane (Liu et al., 2024)	dead-end filtration	0.2–1.6	282	5	20	1–10	>80%
Zr-modified-bentonite membrane (Zhang et al., 2023)	Crossflow filtration	0	940	3–11	20	1–5	20.6 mg.g^{-1}
LDH membrane (Fang et al., 2023)	Dead-end filtration	—	32,337	—	—	2.0	1,146.5 mg·m^{-2}
PVC-LaBT (This work)	Crossflow filtration	0	294	3–11	25	1	244.1 mg·m^{-2}

Notes:
[a]Experimental method.
[b]Temperature.
[c]Initial concentration.
[d]Adsorption capacity.

by 5,000×, 100,00× and 2,000× under a SEM. As can be seen from Figure 2a2,a3, there are few pores with small sizes in pure PVC membranes. These pores are irregular in shape and have thick walls. According to Figure 2a4, when the inner wall of the pores was observed by 200,00×, only a small part of the inner wall has pores with small size, while there are nearly no pores can be found to distribute over most of the inner wall. As can be seen from Figures 2b2–b4, the interior of PVC-BT membrane has a porous mesh structure. These pores are relatively numerous, with small size and irregular shape. Figures 2c2–c4 shows that the interior of PVC-LaBT shows a loose porous structure. The pores have a irregular shape. Compared to the PVC and PVC-BT membranes, the PVC-LaBT membrane has a large internal aperture, wide and dense distribution, and very thin pore walls.

The comparison of SEM images shows that PVC-LaBT has the most internal pores with large size, which indicates that the specific surface area of PVC-LaBT is the largest. Compared to PVC-LaBT, the internal pore size of PVC-BT is smaller. This is because after the modification of bentonite, La^{3+} enters the interlayer of bentonite through ion exchange, increasing the interlayer spacing and improving the specific surface area, resulting in larger membrane pore size. Compared with the composite membrane, the

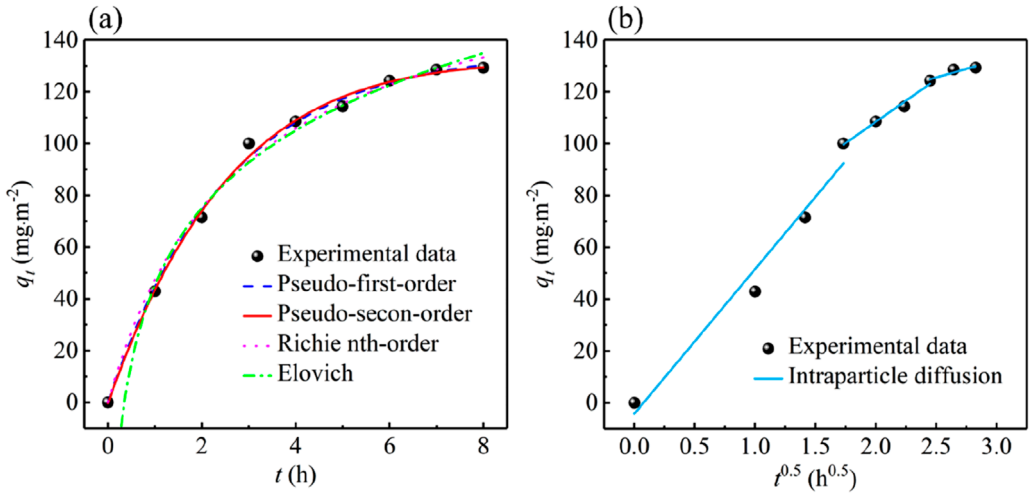

FIGURE 7
Phosphate adsorption kinetic of PVC-LaBT: **(a)** pseudo-first-order, pseudo-second-order, Richie nth-order, Elovich models fitting and **(b)** intraparticle diffusion model fitting.

pores of pure PVC membrane without adding matrix are the least, indicating that the addition of bentonite can improve the specific surface area of the PVC membrane.

3.1.2 AFM characterizations

2D and 3D atomic force microscope (AFM) test images were obtained to observe and compare the surface roughness and morphology of PVC, PVC-BT and PVC-LaBT membranes. The data were analyzed to obtain the parameters of different membrane surface such as average roughness (Ra), maximum height roughness (Rmax) and root mean square roughness (Rq).

According to Figures 3a1, a2, the pure PVC membrane has a smooth surface, with small and uniform surface particles. After PVC AFM data analysis, we obtained its Ra of 8.5 nm, Rq of 10.7 nm and Rmax of 90.3 nm. As can be seen from Figures 3b1, b2, the surface of PVC-BT is relatively rough. Compared with PVC, the surface particles distribute more unevenly. After PVC-BT AFM data analysis, we obtained its Ra of 9.7 nm, Rq of 12.6 nm and Rmax of 122.0 nm. Figures 3c1, c2 shows that the surface of PVC-LaBT is the roughest, which is due to the wide disparity between surface particle sizes. Furthermore, the distribution of surface particles is the most uneven. The AFM data of PVC-LaBT analyzed Ra of 12.2 nm, Rq of 15.7 nm, and Rmax of 170.0 nm. The surface roughness information of PVC, PVC-BT and PVC-LaBT membranes were filled in Table 1 for comparison.

In conclusion, PVC-LaBT has the largest surface roughness, followed by PVC-BT and PVC membranes. According to the comparison of the Ra value of the three membranes, the roughness of PVC-BT is only 14.5% larger than that of pure PVC membrane, while that of PVC-LaBT is 29% higher than that of pure PVC membrane. From this information, it can be inferred that compared to PVC and PVC-BT membranes, PVC-LaBT has the largest specific surface area and the best adsorption performance.

3.2 Pure water flux test

As can be seen from Figure 4, the pure water flux of PVC, PVC-BT and PVC-LaBT are 136, 149 and 294 L·m^{-2}·h^{-1}, respectively. PVC-LaBT has the largest pure water flux, which is about once higher than that of PVC and PVC-BT. This may be due to the enhancement of hydrophilicity, larger porosity and specific surface area of PVC-LaBT. Relevant studies have also yielded similar results (Shen et al., 2024; Pan et al., 2023). The excellent filtration performance of PVC-LaBT contributes to the enrichment and capture of phosphate from aqueous solution.

3.3 Phosphate filtration-adsorption performance

3.3.1 Adsorption properties of different membranes

To compare the performance of different membranes, 1 mg·L^{-1} of phosphate cross flowed through PVC, PVC-BT and PVC-LaBT. The phosphate concentration (C_t) was tested every hour for 8 h. The experimental results are shown in Figure 5.

As can be seen from Figure 5, the three kinds of membranes all have a high phosphate adsorption rate in the first 3 h, among which the adsorption rate of PVC-LaBT was the highest. After 3 h, the C_t of the solution treated by PVC, PVC-BT and PVC-LaBT were 0.75, 0.65 and 0.30 mg·L^{-1} respectively. Since then, the adsorption rate has decreased, and after 7 h, the adsorption process basically entered the adsorption-desorption equilibrium stage. Finally, the C_t of the solution treated by PVC, PVC-BT and PVC-LaBT were 0.70, 0.50 and 0.10 mg·L^{-1} respectively. This is partly because the solubility product constant (pK_{sp}) of La-phosphate is large, which enhances the chemical adsorption, and on the other hand the intercalation of La ions results in larger interlayer space and porosity, thus providing more attachment sites (He et al., 2022).

10.3389/fmats.2025.1596814

TABLE 3 Kinetic model parameters obtained from adsorption.

Kinetic model	Parameter	Value
Pseudo-first-order	k_1 (h^{-1})	0.3954
	$q_{e,cal}$ ($mg{\cdot}m^{-2}$)	136.15
	R^2	0.9967
Pseudo-second-order	k_2 ($m^2{\cdot}mg^{-1}{\cdot}h^{-1}$)	0.0020
	$q_{e,cal}$ ($mg{\cdot}m^{-2}$)	179.97
	R^2	0.9932
Richie nth-order	k_n ($m^{2(n-1)}{\cdot}mg^{1-n}{\cdot}h^{-1}$)	0.3921
	β ($m^2{\cdot}mg^{-1}$)	1.0004
	n	0.8686
	$q_{e,cal}$ ($mg{\cdot}m^{-2}$)	131.73
	R^2	0.9969
Elovich	α ($mg{\cdot}m^{-2}{\cdot}h^{-1}$)	122.9588
	β ($m^2{\cdot}mg^{-1}$)	0.02361
	R^2	0.9923
Intraparticle diffusion	k_{id1} ($mg{\cdot}m^{-2}{\cdot}h^{-0.5}$)	55.7865
	C_1 ($mg{\cdot}m^{-2}$)	−4.2543
	R^2	0.9704
	k_{id2} ($mg{\cdot}m^{-2}{\cdot}h^{-0.5}$)	32.7635
	C_2 ($mg{\cdot}m^{-2}$)	42.8391
	R^2	0.9842
	k_{id3} ($mg{\cdot}m^{-2}{\cdot}h^{-0.5}$)	13.3035
	C_3 ($mg{\cdot}m^{-2}$)	92.2456
	R^2	0.8698

Because SA-LaBT has the best filtration-adsorption performance, it was selected for subsequent influencing factor, adsorption kinetic and isotherm experiments.

3.3.2 Effect of solution pH

Phosphorus-containing wastewater mainly includes municipal sewage, acid pickling and phosphorization wastewater, and wastewater from the phosphorus chemical industry, etc. Their pH values are usually between 3 and 11. To find the effect of solution pH on the filtration-adsorption performance of phosphate by PVC-LaBT. The pH of 1 $mg{\cdot}L^{-1}$ phosphate solution was adjusted with 1 $mol{\cdot}L^{-1}$ HNO_3 solution or NaOH solution to 3, 5, 7, 9 and 11. The filtration-adsorption experiments were performed by using PVC-LaBT and phosphate solution with different pHs. The experimental results are shown in Figure 6a.

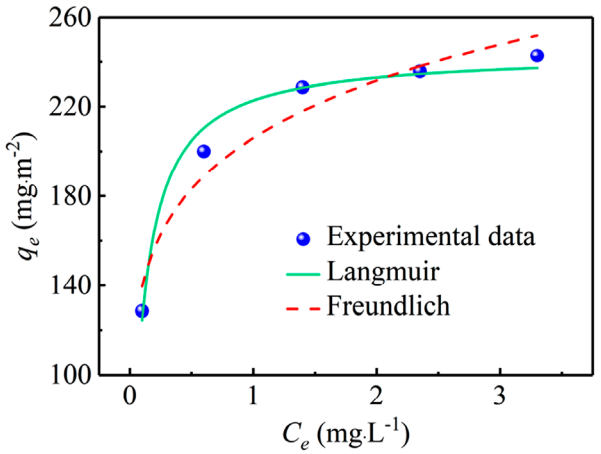

FIGURE 8
Phosphate adsorption isotherm of PVC-LaBT fitting by Langmuir and Freundlich models.

According to Figure 6a, the adsorption capacity of PVC-LaBT was excellent under acidic conditions. The C_t decreased to 0.3 $mg{\cdot}L^{-1}$ and 0.1 $mg{\cdot}L^{-1}$ after 4 h and 8 h, respectively. When solution pH ≥ 7.0, the adsorption capacity of PVC-LaBT weakened with the increment of pH. When the solution was neutral, the C_t decreased to 0.3 $mg{\cdot}L^{-1}$ and 0.2 $mg{\cdot}L^{-1}$ after 4 h and 8 h, respectively. The performance decline was not obvious. However, when pH was 9.0, the adsorption performance decreased rapidly. After 8 h, the C_t decreased only from 1.0 $mg{\cdot}L^{-1}$ to 0.6 $mg{\cdot}L^{-1}$, with the removal efficiency of only 40%. When pH was 11.0, the adsorption performance was completely lost. The reason for the drastic decrement in the performance of PVC-LaBT in the alkaline solution may be caused by the OH^- competing with PO_4^{3-} for the adsorption site (Zhang Y. et al., 2022).

3.3.3 Effect of coexisting anions

To explore the effect of coexisting anions on the performance of phosphate filtration by PVC-LaBT, 0.5 mmol KCl, KNO_3, K_2SO_4 and K_2CO_3 were respectively added to the phosphate solution with a concentration of 1 $mg{\cdot}L^{-1}$. At this time, the molar mass of the coexisting anions in the solution was approximately 70 times the molar mass of the phosphate. The prepared phosphate solution containing coexisting anions passed through PVC-LaBT by cycle cross-flow mode and the C_t was tested after 4 h and 8 h. The experimental results are shown in Figure 6b.

As can be seen from Figure 6b, the order of anion inhibiting phosphate adsorption was: CO_3^{2-}>SO_4^{2-}>Cl^->NO_3^-. After 4 h, the C_t in the blank group decreased to 0.3 $mg{\cdot}L^{-1}$, as was the C_t in the solution containing NO_3^-. The C_t in the solutions containing Cl, SO_4^{2-} and CO_3^{2-} were 0.4 $mg{\cdot}L^{-1}$, 0.5 $mg{\cdot}L^{-1}$ and 0.5 $mg{\cdot}L^{-1}$ respectively. At this point, the inhibitory effect of anions was not obvious. However, after cross flow filtration for 8 h, the C_t in the solutions containing Cl, NO_3^-, SO_4^{2-} and CO_3^{2-} were 0.2 $mg{\cdot}L^{-1}$, 0.1 $mg{\cdot}L^{-1}$, 0.3 $mg{\cdot}L^{-1}$ and 0.5 $mg{\cdot}L^{-1}$ respectively. This shows that divalent anions inhibited phosphate adsorption more strongly, while monovalent anions were less inhibitory. This is because SO_4^- and CO_3^{2-} can complete for adsorption with the phosphate anions.

TABLE 4 Isotherm model parameters obtained from adsorption.

Langmuir model			Freundlich model		
q_m (mg·m^{-2})	K_L (L·mg^{-1})	R^2	K_F (mg$^{(1-1/n)}$·L$^{1/n}$·m^{-2})	n	R^2
244.09	10.40	0.9820	205.95	5.91	0.9493

However, the pK_{sp} between Cl^- or NO_3^- and La_3^- is much smaller than that of PO_4^{3-} and La_3^-, so there is no significant inhibition on the adsorption of phosphate (Du et al., 2022).

3.3.4 Similar membranes comparison

In other studies, adsorbents have also been embedded into organic membranes for the treatment of phosphate. The relevant parameters are listed in Table 2. As can be seen from the table, PVC-LaBT has moderate water flux. It also has outstanding adsorption capacity for phosphate. In addition, PVC-LaBT has the advantages of simple preparation and low cost. Therefore, it is expected to be widely used.

3.4 Adsorption kinetic and isotherm

3.4.1 Adsorption kinetic

In order to explore the adsorption kinetic of PVC-LaBT, the phosphate solution of 1 mg·L^{-1} was recycled through PVC-LaBT. The phosphate concentrations were determined at different times. To understand the mechanisms of adsorption kinetics, the experimental data were fitted with the following five kinetic models (Equations 4–8), (Simonin, 2016; Azizian, 2004; Wang and Guo, 2022):

Pseudo-first-order model:

$$q_t = q_e - q_e e^{-k_1 t} \tag{4}$$

Pseudo-second-order model:

$$q_t = \frac{k_2 q_e^2 t}{1 + k_2 q_e t} \tag{5}$$

Richie nth-order model:

$$q_t = q_e \left\{ 1 - \left[\frac{1}{\beta + k_n (n-1) t} \right]^{\frac{1}{n-1}} \right\} \tag{6}$$

Elovich model:

$$q_t = \frac{1}{\beta} ln(\alpha\beta t) \tag{7}$$

Intraparticle diffusion model:

$$q_t = k_{id} t^{0.5} + C \tag{8}$$

where k_1 (1·h^{-1}), k_2 (m^2·mg^{-1}·h^{-1}) and k_n (m$^{2(n-1)}$·mg^{1-n}·h^{-1}) are the pseudo-first-order equilibrium rate constant, pseudo-second-order equilibrium rate constant and Ritchie nth-order equilibrium rate constant, respectively; n is a fitting parameter, dimensionless and without special significance; α (mg·m^{-2}·h^{-1}) is the adsorption rate at initial time, while β (m^2·mg^{-1}) denotes the constant of desorption. k_{id} (mg·m^{-2}·h$^{-0.5}$) is the rate constant of intraparticle diffusion and C (mg·m^{-2}) is determined by the thickness of boundary layer.

The experimental data fitting results are shown in Figure 7, and the corresponding kinetic parameters are listed in Table 3. As can be seen from Figure 7, in the first 3 h, the phosphate adsorption capacity increased rapidly. In the following 3–6 h, the increment speed of phosphate adsorption capacity became slow. In the next 6–8 h, the adsorption capacity tended to stabilize, and the adsorption process basically reached equilibrium.

The parameters listed in Table 3 show that the Pseudo-first-order, Pseudo-second-order, Richie nth-order and Elovich models all have high R^2 values, among which the Richie nth-order model has the highest R^2 coefficient (0.9969), indicating that the adsorption of phosphate by PVC-LaBT is controlled by various mechanisms, including chemical adsorption, electrostatic attraction, hydrogen bonding and outer-sphere complex formation (Pan W. et al., 2022). Moreover, the theoretical adsorption capacity calculated by the Richie nth-order model (131.73 mg·m^{-2}) basically agrees with the experimental adsorption capacity value (129.29 mg·m^{-2}).

Furthermore, to elucidate the diffusion mechanism of phosphate during adsorption, the kinetic data were fitted to Intraparticle diffusion model with three linear regions. The data are shown in Figure 7b and Table 3. This plot exhibits a multilinear morphology that can be divided into three linear regions, suggesting that intra-particle diffusion is not the only rate-control step for the entire reaction (Luo et al., 2021). The k_{id1} value was 55.7865 mg·m^{-2}·h$^{-0.5}$, indicating that the adsorption rate is the highest in the first stage, during which the phosphate ions were adsorbed to the surface PVC-LaBT. The slope of the second linear region decreased, with k_{id2} value being 32.7635 mg·m^{-2}·h$^{-0.5}$, demonstrating that the adsorption rate at this stage was controlled by intra-particle or pore diffusion. The last linear region flattened out, exhibiting the last equilibrium phase.

3.4.2 Adsorption isotherm

The isotherm experiments were performed by putting PVC-LaBT in the triple high pressure plate membrane testing equipment and cycle the phosphate solution of different initial concentrations (1, 2, 3, 4 and 5 mg·L^{-1}). The phosphate concentrations were tested after 20 h, and thus the phosphate adsorption capacities were calculated. At last, the experimental data were fitted with Langmuir and Freundlich models using Equations 9, 10 respectively listed below, in order to analyze the adsorption mechanism and predict the maximum adsorption capacity (Wang and Guo, 2020; Foo and Hameed, 2010).

Langmuir model:

$$q_e = \frac{q_m K_L C_e}{1 + K_L C_e} \tag{9}$$

Freundlich model:

$$q_e = K_F C_e^n \tag{10}$$

where K_L ($L \cdot mg^{-1}$) and K_F ($mg^{(1-1/n)} \cdot L^{1/n} \cdot m^{-2}$) are the Langmuir adsorption equilibrium constant and the affinity parameter of Freundlich model respectively; q_m ($mg \cdot m^{-2}$) indicates the Langmuir maximum adsorption capacity; n is the Freundlich linearity constant.

According to Figure 8, the phosphate adsorption capacity of PVC-LaBT is gradually increased as the initial phosphate concentration increased from 1 $mg \cdot L^{-1}$ to 5 $mg \cdot L^{-1}$. The obtained isotherm parameters are tabulated in Table 4. The fitting degree of the model is mainly based on the value of R^2. Generally, the higher the value of R^2 indicates the better a fit is. Table 4 shows that the Langmuir model gives a high correlation coefficient R^2 (0.9820), indicating that the adsorption system was mainly monolayer and the phosphate ions dispersed uniformly on the active sites of PVC-LaBT without interaction (Abukhadra and Mostafa, 2019). However, the Freundlich model (R^2 = 0.9493) is not negligible. This indicates that there is also a multi-layer adsorption phenomenon with heterogeneous surfaces in the PVC-LaBT. That is to say, a portion of the adsorption active sites on the PVC-LaBT surface are unevenly distributed, which can lead to the phenomenon of active site stacking (Wang L. et al., 2023). Furthermore, the maximum adsorption capacity of PVC-LaBT predicted by Langmuir model was 244.09 $mg \cdot m^{-2}$.

4 Conclusion

In this study, PVC-LaBT was prepared by chemical precipitation and phase conversion method for low concentration of phosphate removal. Compared with other adsorbents, PVC-LaBT has the advantages of low cost, simple preparation, high adsorption capacity, high selectivity and easy recovery. The pure water flux of PVC-LaBT is 294 $L \cdot m^{-2} \cdot h^{-1}$, much higher than that of PVC and PVC-BT. Using 1 $mg \cdot L^{-1}$ phosphate solution, after treatment of 8 h by PVC-LaBT, phosphate concentration decreased to 0.1 $mg \cdot L^{-1}$. The adsorption process was favored in both neutral and acidic water environments. Coexist anions have limited influence on the adsorption properties. Adsorption kinetic models fitting shows that the adsorption process was controlled by different mechanisms. Adsorption isotherms can be better fitted with Langmuir model, indicating the adsorption process is monolayer and uniform, with the maximum adsorption capacity of 244.09 $mg \cdot m^{-2}$. PVC-LaBT is expected to be useful in low-concentration phosphate wastewater.

Data availability statement

The original contributions presented in the study are included in the article/supplementary material, further inquiries can be directed to the corresponding author.

Author contributions

HX: Conceptualization, Formal Analysis, Funding acquisition, Methodology, Writing – original draft, Writing – review and editing. XC: Data curation, Investigation, Writing – review and editing. TS: Resources, Funding acquisition, Writing – review and editing. LC: Supervision, Investigation, Writing – review and editing.

Funding

The author(s) declare that financial support was received for the research and/or publication of this article. The authors would like to acknowledge the financial support from the Basic Science (Natural Science) Research Project of Jiangsu institutions of higher education (23KJB430023) and the research project of Nanjing Vocational Institute of Transport Technology (JZ2308).

Conflict of interest

The authors declare that the research was conducted in the absence of any commercial or financial relationships that could be construed as a potential conflict of interest.

Generative AI statement

The author(s) declare that no Generative AI was used in the creation of this manuscript.

Publisher's note

References

Abukhadra, M. R., and Mostafa, M. (2019). Effective decontamination of phosphate and ammonium utilizing novel muscovite/phillipsite composite; equilibrium investigation and realistic application. *Sci. Total Environ.* 667, 101–111. doi:10.1016/j.scitotenv.2019.02.362

Ahmadijokani, F., Molavi, H., Rezakazemi, M., Tajahmadi, S., Bahi, A., Ko, F., et al. (2022). UiO-66 metal-organic frameworks in water treatment: a critical review. *Prog. Mater. Sci.* 125, 100904. doi:10.1016/j.pmatsci.2021.100904

Azizian, S. (2004). Kinetic models of sorption: a theoretical analysis. *J. Colloid Interface Sci.* 276 (1), 47–52. doi:10.1016/j.jcis.2004.03.048

Di Capua, F., De Sario, S., Ferraro, A., Petrella, A., Race, M., Pirozzi, F., et al. (2022). Phosphorous removal and recovery from urban wastewater: current practices and new directions. *Sci. Total Environ.* 823, 153750. doi:10.1016/j.scitotenv.2022.153750

Dithmer, L., Nielsen, U. G., Lundberg, D., and Reitzel, K. (2016). Influence of dissolved organic carbon on the efficiency of P sequestration by a lanthanum modified clay. *Water Res.* 97, 39–46. doi:10.1016/j.watres.2015.07.003

Du, M., Zhang, Y., Wang, Z., Lv, M., Tang, A., Yu, Y., et al. (2022). Insight into the synthesis and adsorption mechanism of adsorbents for efficient phosphate removal: exploration from synthesis to modification. *Chem. Eng. J.* 442, 136147. doi:10.1016/j.cej.2022.136147

Fang, D., Huang, L., Xiao, H., Wu, G., Zeng, Z., Wang, X., et al. (2023). Layered double hydroxide membranes for advanced removal of phosphate from wastewater. *Chem. Eng. J.* 451, 138600. doi:10.1016/j.cej.2022.138600

Foo, K. Y., and Hameed, B. H. (2010). Insights into the modeling of adsorption isotherm systems. *Chem. Eng. J.* 156 (1), 2–10. doi:10.1016/j.cej.2009.09.013

Haciosmanoglu, G. G., Mejias, C., Martin, J., Santos, J. L., Aparicio, I., and Alonso, E. (2022). Antibiotic adsorption by natural and modified clay minerals as designer adsorbents for wastewater treatment: a comprehensive review. *J. Environ. Manag.* 317, 115397. doi:10.1016/j.jenvman.2022.115397

He, L., Chen, Y., Sun, F., Li, Y., Huang, W., and Yang, S. (2022). Controlled release of phosphorus using lanthanum-modified hydrochar synthesized from water treatment sludge: adsorption behavior and immobilization mechanism. *J. Water Process Eng.* 50, 103319. doi:10.1016/j.jwpe.2022.103319

Hnamte, M., and Pulikkal, A. K. (2022). Clay-polymer nanocomposites for water and wastewater treatment: a comprehensive review. *Chemosphere* 307, 135869. doi:10.1016/j.chemosphere.2022.135869

Jia, X., Wang, H., Li, Y., Xu, J., Cheng, H., Li, M., et al. (2022). Separable lanthanum-based porous PAN nanofiber membrane for effective aqueous phosphate removal. *Chem. Eng. J.* 433, 133538. doi:10.1016/j.cej.2021.133538

Liu, G., Wei, N., Wu, W., Liu, Q., Wang, Y., Du, K., et al. (2024). Preparation of a novel LC@MWCNTs membrane and its application for enhanced phosphate removal and fouling control. *J. Water Process Eng.* 64, 105644. doi:10.1016/j.jwpe.2024.105644

Liu, S., Zhao, S., Fan, F., Zhang, B.-T., and Wang, S. (2022). Magnetically separable and recyclable lanthanum/iron co-modified attapulgite: a sustainable option to efficiently control phosphate loading. *J. Clean. Prod.* 348, 131294. doi:10.1016/j.jclepro.2022.131294

Luo, H., Wang, Y., Wen, X., Cheng, S., Li, J., and Lin, Q. (2021). Key roles of the crystal structures of MgO-biochar nanocomposites for enhancing phosphate adsorption. *Sci. Total Environ.* 766, 142618. doi:10.1016/j.scitotenv.2020.142618

Mi, X., Yu, F., Zhang, H., Chen, R., Hu, X., Zhang, W., et al. (2022). Lanthanum activated palygorskite for selective phosphate separation from aqueous media: comprehensive understanding of adsorptive behavior and mechanism affected by interfering substances. *Chem. Eng. J.* 443, 136423. doi:10.1016/j.cej.2022.136423

Pan, W., Liu, X., Yang, P., and Han, R. (2022b). Use of iron-crosslinked sodium alginate beads for adsorption of phosphate from solution. *Desalination Water Treat.* 272, 108–117. doi:10.5004/dwt.2022.28848

Pan, Y., Huang, W., Zhou, Y., Liu, F., Zhu, C., Pang, H., et al. (2023). Covalent-crosslinking IRMOF-3-NH_2/PVC ultrafiltration membrane for simultaneous removal of bisphenol A and Cd^{2+} ions in water. *J. Clean. Prod.* 403, 136868. doi:10.1016/j.jclepro.2023.136868

Pan, Y., Liu, F., Zhou, Y., Zhu, C., Pang, H., and Xu, B. (2022a). Defect-rich covalently-crosslinked UiO-66(Zr)-NH_2/PVC adsorption ultrafiltration membrane for effective phosphate ions removal from water. *J. Taiwan Inst. Chem. Eng.* 141, 104575. doi:10.1016/j.jtice.2022.104575

Radoor, S., Jayakumar, A., Shivanna, J. M., Karayil, J., Kim, J. T., and Siengchin, S. (2025). Adsorptive removal of crystal violet from aqueous solution by bioadsorbent. *Biomass Convers. Biorefinery* 15 (2), 2431–2442. doi:10.1007/s13399-023-05079-8

Radoor, S., Kassahun, S. K., and Kim, H. (2024). Selective adsorption of cationic dye by κ-carrageenan-potato starch bio-hydrogel: kinetics, isotherm, and thermodynamic studies. *Int. J. Biol. Macromol.* 281, 136377. doi:10.1016/j.ijbiomac.2024.136377

Rangabhashiyam, S., Dos Santos Lins, P. V., De Magalhaes Oliveira, L. M. T., Sepulveda, P., Ighalo, J. O., Rajapaksha, A. U., et al. (2022). Sewage sludge-derived biochar for the adsorptive removal of wastewater pollutants: a critical review. *Environ. Pollut.* 293, 118581. doi:10.1016/j.envpol.2021.118581

Sabarish, R., and Unnikrishnan, G. (2018). Polyvinyl alcohol/carboxymethyl cellulose/ZSM-5 zeolite biocomposite membranes for dye adsorption applications. *Carbohydr. Polym.* 199, 129–140. doi:10.1016/j.carbpol.2018.06.123

Sabarish, R., and Unnikrishnan, G. (2019). Synthesis, characterization and evaluations of micro/mesoporous ZSM-5 zeolite using starch as bio template. *SN Appl. Sci.* 1, 989–13. doi:10.1007/s42452-019-1036-9

Shen, D., Ma, H., Khan, M., and Hsiao, B. S. (2024). Highly efficient and sustainable cationic polyvinyl chloride nanofibrous membranes for removal of *E. coli* and Cr (VI): filtration and adsorption. *Chem. Eng. J.* 479, 147269. doi:10.1016/j.cej.2023.147269

Simonin, J.-P. (2016). On the comparison of pseudo-first order and pseudo-second order rate laws in the modeling of adsorption kinetics. *Chem. Eng. J.* 300, 254–263. doi:10.1016/j.cej.2016.04.079

Wang, B., Zhang, H., Hu, X., Chen, R., Guo, W., Wang, H., et al. (2023a). Efficient phosphate elimination from aqueous media by La/Fe bimetallic modified bentonite: adsorption behavior and inner mechanism. *Chemosphere* 312, 137149. doi:10.1016/j.chemosphere.2022.137149

Wang, J., and Guo, X. (2020). Adsorption isotherm models: classification, physical meaning, application and solving method. *Chemosphere* 258, 127279. doi:10.1016/j.chemosphere.2020.127279

Wang, J., and Guo, X. (2022). Rethinking of the intraparticle diffusion adsorption kinetics model: interpretation, solving methods and applications. *Chemosphere* 309, 136732. doi:10.1016/j.chemosphere.2022.136732

Wang, L., Wang, L., and Li, L. (2023b). Preparation of PVC-LMZO membrane and its lithium adsorption performance from brine. *Desalination* 561, 116689. doi:10.1016/j.desal.2023.116689

Xi, H., Min, F., Yao, Z., and Zhang, J. (2023). Facile fabrication of dolomite-doped biochar/bentonite for effective removal of phosphate from complex wastewaters. *Front. Environ. Sci. and Eng.* 17 (6), 71. doi:10.1007/s11783-023-1671-7

Zhang, A., Fang, S., Ge, M., Zhang, J., Xi, H., Xu, Y., et al. (2024). Microalgae-derived hydrogels/membranes for phosphorus removal and recovery from aquaculture tailwater: waste utilization and phosphorus recycling. *Bioresour. Technol.* 409, 131246. doi:10.1016/j.biortech.2024.131246

Zhang, A., Fang, S., Xi, H., Huang, J., Li, Y., Ma, G., et al. (2023). Highly efficient and selective removal of phosphate from wastewater of sea cucumber aquaculture for microalgae culture using a new adsorption-membrane separation-coordinated strategy. *Front. Environ. Sci. and Eng.* 17 (10), 120. doi:10.1007/s11783-023-1720-2

Zhang, C., Guisasola, A., and Antonio Baeza, J. (2022a). A review on the integration of mainstream P-recovery strategies with enhanced biological phosphorus removal. *Water Res.* 212, 118102. doi:10.1016/j.watres.2022.118102

Zhang, M., He, M., Chen, Q., Huang, Y., Zhang, C., Yue, C., et al. (2022b). Feasible synthesis of a novel and low-cost seawater-modified biochar and its potential application in phosphate removal/recovery from wastewater. *Sci. Total Environ.* 824, 153833. doi:10.1016/j.scitotenv.2022.153833

Zhang, Y., Yang, K., Fang, Y., Ding, J., and Zhang, H. (2022c). Removal of phosphate from wastewater with a recyclable La-based particulate adsorbent in a small-scale reactor. *Water* 14 (15), 2326. doi:10.3390/w14152326